Correspondence to:
R. Wang and Q. Lu,
rswan@ustc.edu.cn;
qmlu@ustc.edu.cn

Large-Scale Parallel Electric Field Colocated in an Extended Electron Diffusion Region During the Magnetosheath Magnetic Reconnection

Shimou Wang[1,2,3] ![ORCID], **Rongsheng Wang**[1,2,3] ![ORCID], **Quanming Lu**[1,2,3] ![ORCID], **C. T. Russell**[4] ![ORCID], **R. E. Ergun**[5] ![ORCID], and **Shui Wang**[1,2,3]

[1]CAS Key Laboratory of Geospace Environment, Department of Geophysics and Planetary Science, School of Earth and Space Sciences, University of Science and Technology of China, Hefei, China, [2]CAS Center for Excellence in Comparative Planetology, Hefei, China, [3]Anhui Mengcheng Geophysics National Observation and Research Station, University of Science and Technology of China, Mengcheng, China, [4]Earth Planetary and Space Sciences, University of California Los Angeles, Los Angeles, CA, USA, [5]Laboratory of Atmospheric and Space Sciences, University of Colorado, Boulder, CO, USA

Abstract   In this study, we report observations from the Magnetospheric Multiscale (MMS) mission of large-scale parallel electric fields in a magnetosheath reconnecting current sheet. The four MMS satellites successively crossed an electron jet embedded in a broad current sheet and detected a unipolar $E_\parallel$ being colocated with the jet. The strong electron pressure anisotropy inside the broad current sheet suggests that the jet could be generated by the firehose instability. The observations show that the large-amplitude $E_\parallel$ can fill the entire electron diffusion region (EDR) in the magnetosheath reconnection and thus dominates electron acceleration therein, dramatically different from EDRs in the magnetotail and magnetopause where large-amplitude unipolar $E_\parallel$ was rarely detected. The appearance of this $E_\parallel$ could be due to the strong guide field which is common in the magnetosheath.

Plain Language Summary   Magnetic reconnection is a fundamental physical process in space and astrophysical plasmas in which magnetic energy is converted into plasma kinetic energy and heat. Magnetic reconnection is believed to be initiated in a small-scale electron diffusion region (EDR) where electrons are decoupled from the magnetic field lines. Recent spacecraft observations in Earth's magnetosheath have revealed a new form of magnetic reconnection without ion coupling in electron-scale current sheets. The detailed properties of the EDR in these electron-only reconnection events have been scarce. In this letter, we report Magnetospheric Multiscale mission observations of large-amplitude and unipolar parallel electric fields being colocated with the EDR of a magnetosheath reconnecting current sheet. The parallel electric field has a large spatial extent that fills the entire EDR. This parallel electric field generates a potential drop of 120 V, which can accelerate electrons passing through the EDR. Altogether, our results suggest that large-scale parallel electric fields can dominate the electron dynamics in the EDR of magnetosheath electron-only reconnection events that usually have large guide fields.

1. Introduction

Magnetic reconnection is a universal plasma process in space and astrophysical environment that can convert magnetic energy into plasma kinetic and thermal energy (Hesse and Cassak, 2020; Yamada et al., 2010). The magnetosheath, downstream of the bow shock, is a turbulent plasma environment with many small-scale current sheets (CSs) where magnetic reconnection is easily initiated (Karimabadi et al., 2014; Lu et al., 2020; Retino et al., 2007; Wang et al., 2021). These CSs are generally thin, with short durations of a few seconds or less when passing a spacecraft. Thus, high-resolution data, especially plasma data, are needed to explore the electron physics inside these CSs. Recent spacecraft observations by Magnetospheric Multiscale (MMS) mission (Burch, Moore, et al., 2016) have reported signatures of ion diffusion regions (IDRs) and electron diffusion regions (EDRs) in magnetosheath CSs (Voros et al., 2017; Yordanova et al., 2016). These characteristics are similar to the reconnection events observed at the magnetopause (Burch, Torbert, et al., 2016; Wang et al., 2017) and in the magnetotail (Li et al., 2019; Torbert et al., 2018; R. S. Wang et al., 2020).

In the magnetosheath, an important feature of EDR is the parallel electric field $E_\parallel$ (Phan et al., 2018; Wilder et al., 2018). The $E_\parallel$ structure is observed within a high-speed electron jet outside the reconnection EDR and

causes strong energy dissipation (Wilder et al., 2017). Further study shows that $E_\parallel$ becomes increasingly important for energy dissipation in reconnection with increasing guide fields (Wilder et al., 2018). The large-amplitude $E_\parallel$ was also reported inside the EDR at the flank magnetopause (Eriksson et al., 2016). Ergun, Goodrich, et al. (2016) interpreted the strong $E_\parallel$ events as the result of secondary reconnection inside flux ropes (S. M. Wang et al., 2020). Because of the guide field in reconnection, the $E_\parallel$ would be created inside the diffusion region and significantly affects the particle dynamics (Drake et al., 2005; Huang et al., 2010; Pritchett and Coroniti, 2004; Ricci et al., 2004; Swisdak et al., 2005). Recent simulations show that the EDRs fall into different regimes depending on the guide field and the electron β (Le et al., 2013). An extended EDR embedded in the reconnection exhaust, called "Regime III" EDR, was produced by the firehose instability in the simulations with normalized guide fields in the range of 0.15–0.6 (Le et al., 2013), which has not been verified by the spacecraft data. Furthermore, the relation between the $E_\parallel$ and EDR remains to be studied.

In this work, we studied a magnetosheath reconnecting CS with a strong unipolar $E_\parallel$. This event was first reported by Wilder et al. (2018) and selected as an example of the high guide field reconnection event to compare with the other two events with smaller guide fields. Wilder et al. (2018) mainly investigated the role of $E_\parallel$ in energy dissipation and compared the agyrotropic electron distributions in the presence of different guide fields. Here, we focused on the structure of the EDR and quantitatively studied the effect of $E_\parallel$ on the electron distributions by the electron data in the highest time resolution of 7.5 ms resolution (Rager et al., 2018). The large-amplitude unipolar $E_\parallel$ was observed inside the EDR by four MMS spacecraft, indicating that the $E_\parallel$ structure had a spatial extent larger than the spacecraft separation and can fill the entire EDR. This large-scale $E_\parallel$ structure around reconnection X-line is rare in previous spacecraft observations.

2. Data and Instrumentation

We used magnetic field data from Fluxgate Magnetometer (Russell et al., 2016) sampled at 128/s, electric field data from Electric Double Probes (Ergun, Tucker, et al., 2016; Lindqvist et al., 2016) sampled at 8192/s, and plasma distributions and moments data from Fast Plasma Investigation (Pollock et al., 2016) with 30-ms electron cadence and 150-ms ion cadence. Due to the short duration of $E_\parallel$ inside the EDR ($\sim$40 ms), we used the plasma data with higher time resolution (7.5 ms for electrons and 37.5 ms for ions), obtained by reducing the azimuthal sampling resolution (Rager et al., 2018).

3. CS in the Magnetosheath

In the interval of 04:34:20-04:36:15 UT on 04 November 2015, four MMS spacecraft were located in the Earth's magnetosheath at (10.2, 1.9, −0.4) R_E in geocentric solar ecliptic (GSE) coordinates. During the interval, the large magnetic field fluctuations were identified as flux ropes associated with thin CSs (Wang et al., 2021). This letter mainly focused on the CS with the strongest current (larger than 8 μA/m^2). The observations are presented in the CS boundary normal (LMN) coordinates. We determined the LMN coordinates as follows: $\mathbf{M} = \left(\mathbf{B_1} \times \mathbf{B_2}\right) \times \left(\mathbf{B_1} - \mathbf{B_2}\right)/\left|\left(\mathbf{B_1} \times \mathbf{B_2}\right) \times \left(\mathbf{B_1} - \mathbf{B_2}\right)\right|$, along the X-line direction; $\mathbf{N} = \left(\mathbf{B_1} \times \mathbf{B_2}\right)/\left|\mathbf{B_1} \times \mathbf{B_2}\right|$, along the CS normal; and $\mathbf{L} = \mathbf{M} \times \mathbf{N}$, along the reconnecting magnetic field direction. Here, $\mathbf{B_1} = \left(-45.5, 31.1, 45.5\right)_{GSE}$ (nT) and $\mathbf{B_2} = \left(-8.5, -36.6, 31.0\right)_{GSE}$ (nT) are average magnetic fields at two boundaries of CS observed at MMS3. The timing method (Schwartz, 1998) was performed to the points of $B_L = 0$, and the speed of CS was calculated to be 206.1 km/s along the normal direction.

Figure 1 presents the CS observed by MMS1. Based on the magnetic field, electric field, and current density variations, an EDR was identified within the shaded region. The duration of EDR crossing is approximately 40 ms. Then, its width is 8.2 km ($\sim$11.7 d_e). Here, d_e ($\sim$0.7 km) is the electron inertial length and is calculated using number density at the CS center.

Inside the CS (04:35:07.0–04:35:07.5 UT), MMS1 observed a broad electron spectrogram and acceleration at the energy $\sim$200 eV (Figure 1a). Across the EDR (shaded region), B_L presented a sharp rotation from $\sim$50 to $\sim$−20 nT, B_M had a significant decrease, and B_N had a positive value of $\sim$10 nT therein (Figure 1b). Magnetic field strength and plasma density (Figure 1c) on two sides of the CS both exhibited asymmetries, like magnetopause reconnection events (Burch, Torbert, et al., 2016; Wang et al., 2017). No ion jet (not shown) was observed within the CS. Different from ion flows, inside the EDR, electron flows had a negative enhancement in V_{eL},
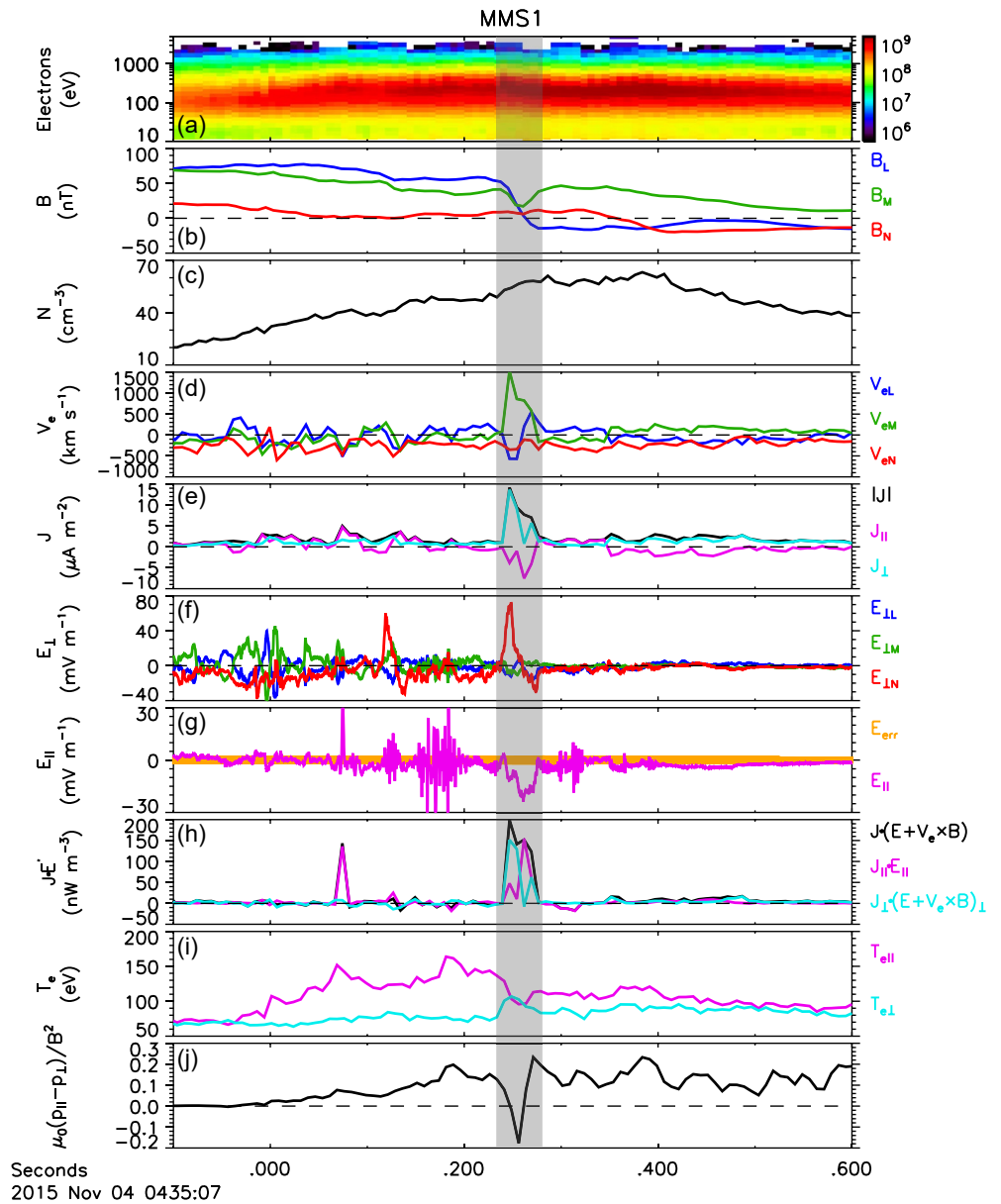
Figure 1. Overview of the current sheet observed by Magnetospheric Multiscale 1. (a) Electron energy-time spectrogram (color scale, in units of keV cm^{-2} s^{-1} sr^{-1} keV^{-1}), (b) magnetic field, (c) electron number density, (d) electron flow, (e) current density and its parallel and perpendicular components, (f) perpendicular electric field, (g) parallel electric field, (h) $\mathbf{J} \cdot \mathbf{E}' = \mathbf{J} \cdot \left(\mathbf{E} + \mathbf{V}_e \times \mathbf{B} \right)$ and its parallel and perpendicular components, (i) electron temperature, and (j) firehose instability parameter $\mu_0 \left(p_\parallel - p_\perp \right)/B^2$. The shaded region represents the electron diffusion region.

~-500 km/s (Figure 1d), larger than local ion Alfvén speed (200 km/s). The decoupling of the $\mathbf{V}_i$ and $\mathbf{V}_e$ caused a Hall current, which is also consistent with the decrease of Hall magnetic field B_M. Figure 1e shows the current density $|\mathbf{J}|$ (black curve), the parallel (pink), and perpendicular (cyan) components. The $J_\perp$ had an obvious enhancement (~15 μA/m^2) inside the EDR. The $J_\parallel$ reversed from positive to negative when approaching the EDR from the inflow region.

Figures 1f and 1g show the perpendicular and parallel electric fields, respectively. A remarkable feature is the asymmetric bipolar Hall electric field with a larger amplitude (~70 mV/m) on the side with larger $|\mathbf{B}|$. Simultaneously, a unipolar $E_\parallel$ reaching ~-20 mV/m was observed inside the whole EDR, indicating that $E_\parallel$ is widely distributed therein. According to the $E_\parallel$ profile (04:35:07.24–04:35:07.28 UT), an electric potential of ~118 V

was obtained. Another important feature is that, outside the EDR, electric fields had stronger fluctuations and larger amplitudes in the inflow region with $B_L > 0$. Figure 1h shows the energy conversion from the electromagnetic field to plasmas in the electron rest frame $\mathbf{J} \cdot \mathbf{E}'$, where $\mathbf{E}' = \mathbf{E} + \mathbf{V_e} \times \mathbf{B}$. $\mathbf{J} \cdot \mathbf{E}'$ was largely positive inside the EDR, suggesting that magnetic energy was converted into plasma energy. Both the parallel and perpendicular components had an important role in energy dissipation. At ∼04:35:07.0 UT, the parallel and perpendicular electron temperature ($T_{e\parallel}$ and $T_{e\perp}$) began to separate (Figure 1i), which suggests that MMS was crossing the reconnection separator here. Correspondingly, on the other side of the CS with $B_L < 0$, MMS exited the exhaust at ∼04:35:07.5 UT where B_L and B_M settle into more asymptotic values, and $T_{e\parallel}$ is almost equal to $T_{e\perp}$ afterward. Thus, the width of the exhaust along the normal direction is ∼103.1 km (∼147.3 d_e). Like in Phan et al. (2007), this suggests that MMS observed the EDR to extend far downstream from the X-line. In the center of the EDR, electron temperature anisotropy $T_{e\parallel}/T_{e\perp}$ is small (∼0.9) compared with the maximal $T_{e\parallel}/T_{e\perp}$ (∼2.0) observed near left edge of the EDR (Figure 1i). Asymmetric reconnection simulations with high guide fields have shown that strong electron temperature anisotropy (∼2.0) in the exhaust can generate thin CS, especially for weak asymmetry case (Montag, 2018). To check the firehose instability condition, Figure 1j presents parameter $\mu_0 \left(p_\parallel - p_\perp \right)/B^2$ and this parameter has a maximum (>0.2) near the edge of the EDR.

In summary, MMS crossed an EDR embedded in a much broader reconnection exhaust. The EDR is characterized by the intense out-of-plane current, super-Alfvénic electron outflow, $E_\parallel$, and $\mathbf{J} \cdot \mathbf{E}' > 0$. The width of the exhaust is ∼103.1 km (∼147.3 d_e), much broader than the EDR width (∼11.7 d_e). The strong electron pressure anisotropy in the exhaust suggests that the current inside the EDR could be generated by the firehose instability.

4. Spatial Variations of $E_\parallel$ and Electron Flows Inside EDR

4.1. Magnetic Fields and Electron Flows

Figures 2a–2d show observations of magnetic fields in the CS observed by MMS1-4. Comparing the B_L at four spacecraft (Figure 2b), a reversal was observed by MMS3, MMS2, MMS4, and MMS1 in turn. This suggests that spacecraft crossed the CS in the + **N** direction with a speed of ∼206.1 km/s calculated by the timing method. This speed is comparable to the magnetosheath ion flow V_{iN} (not shown), suggesting the ion bulk flow carried CS across the spacecraft. Inside the EDR, for MMS2-4, the B_L profile shows a sharper rotation on the $B_L > 0$ side and a subsequent smoother variation on the $B_L < 0$ side, while for MMS1, it presents a sharp rotation across the whole EDR. Note that when MMS2 crossed the midplane ($B_L = 0$) of the EDR, MMS1 just entered the EDR edge (Figure 2b). It suggests that the half-thickness of EDR is about equal to the separation of MMS2 and MMS1 in the **N** direction (∼5.0 km; Figure 2i), which is comparable to the half-thickness calculated by the timing method (4.1 km).

The B_M profile shows a dip, consistent with the unipolar Hall magnetic field, inside the EDR. MMS2 observed the weakest Hall magnetic field, while MMS1 and MMS3 observed the largest. The normal magnetic field B_N was almost zero across the EDR for MMS2-4, except for MMS1, which observed a significant positive B_N (∼10 nT; Figure 2d). The enhancement of ∼10 nT in B_N suggests that MMS1 crossed the newly reconnected field lines. Small B_N observed by MMS2-4 indicates that they were closer to the X-line. The B_N distributions are also consistent with the four spacecraft locations in the **L** direction as shown in Figures 2i and 2j, where MMS1 was farthest from the other three spacecraft in the − **L** direction, with a distance of 19.4 km away from MMS2. Thus, the EDR was detected at a distance of >19.4 km (27.7 d_e) downstream of the X-line. The aspect ratio of this elongated EDR is smaller than 0.2 (<N/L ∼8.2 km/38.8 km).

As shown in Figure 1, the current inside EDR was mainly carried by the electrons. To see the Hall current system more clearly, the perpendicular electron velocity in the **L** direction $V_{e\perp L}$ was calculated in Figure 2e. Note that $V_{e\perp L}$ was small outside the EDR and showed a bipolar variation from negative to positive inside the EDR. This reversed electron jet in the **L** direction corresponded to the electron outflow (negative) and inflow (positive) as shown in Figure 2k, and induced a decreased Hall magnetic field B_M. Inside the EDR, four spacecraft observed fast out-of-plane electron flows $V_{e\perp M}$ (Figure 2f) that produced the main current J_M and associated rapid reversal of B_L. Parallel electron flows $V_{e\parallel}$ (Figure 2g) generally had positive values inside the EDR. In the inflow region with $B_L > 0$, $V_{e\parallel}$ had stronger fluctuations that coincided with $E_\parallel$ therein. Figure 2h plots $\mathbf{J} \cdot \mathbf{E}'$, showing large values inside the EDR. MMS1 observed the largest $\mathbf{J} \cdot \mathbf{E}'$ while MMS2-4 observed smaller $\mathbf{J} \cdot \mathbf{E}'$ values, indicating inhomogeneous distributions of $\mathbf{J} \cdot \mathbf{E}'$ inside the EDR.
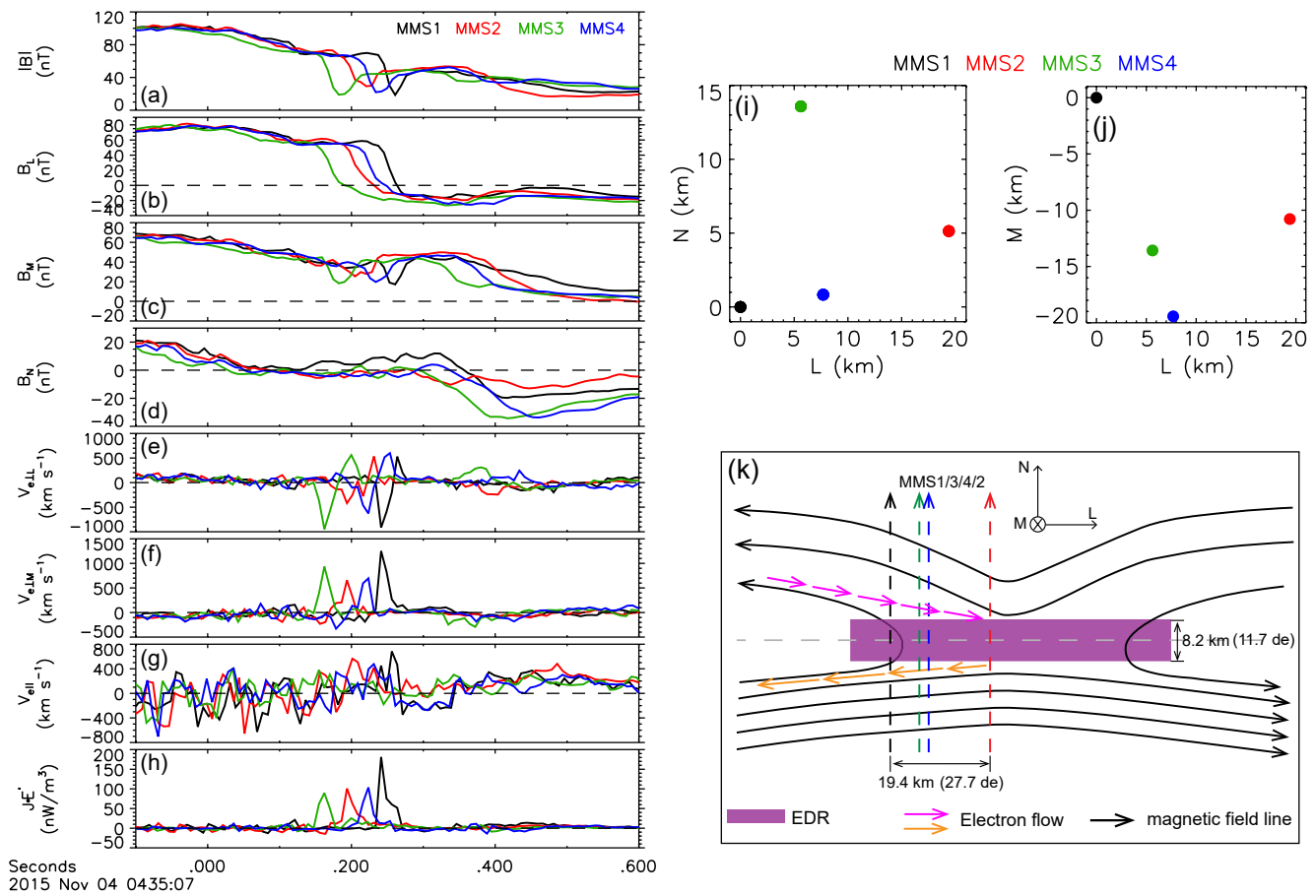
Figure 2. Multi-spacecraft observations of the current sheet. (a–d) Magnitude and components of magnetic field, (e and f) L and M components of the perpendicular electron flows, (g) parallel electron flows, (h) $\mathbf{J} \cdot \mathbf{E}' = \mathbf{J} \cdot \left(\mathbf{E} + \mathbf{V_e} \times \mathbf{B}\right)$, (i and j) location of four Magnetospheric Multiscale (MMS) spacecraft in the L-N and L-M plane, and (k) a schematic illustration for reconnecting current sheet.

4.2. Parallel Electric Fields

In this subsection, we focus on the spatial distributions of the $E_\parallel$, especially the unipolar $E_\parallel$ and its role. To make each curve representing $E_\parallel$ observations by different spacecraft visible (Figures 3b and 3c), the zero lines were shifted by 30 mV/m for MMS1 and 15 mV/m for MMS4. Four spacecraft observed unipolar $E_\parallel$ one by one during the whole EDR crossing, although with different durations and amplitudes, indicating that $E_\parallel$ structure had a spatial extent larger than the spacecraft separation and may fill the entire EDR. MMS2 observed the weakest $E_\parallel$ (~-10 mV/m), while MMS1 observed the strongest $E_\parallel$ (~-25 mV/m). Additionally, the unipolar $E_\parallel$ exhibited two dips, and two dips along spacecraft trajectories were different. For example, between 04:35:07.24 and 04:35:07.25 UT, MMS1 observed the first $E_\parallel$ dip that was mainly along the $\mathbf{L}$ direction (Figure 3d). Immediately, MMS1 observed another dip (04:35:07.25–04:35:07.28 UT) that corresponded with a $E_{M\parallel}$ dip in Figure 3d. In contrast, for MMS2-4, two dips of $E_\parallel$ were mainly contributed from the $E_{M\parallel}$ ($E_{L\parallel}$ and $E_{M\parallel}$ from MMS4 are shown in Figure 3e), and the boundary of two dips just corresponded with the $B_L = 0$ plane where $\left|\mathbf{B}\right| \approx B_M$. Thus, the $E_\parallel$ was almost equal to the reconnection electric field E_M at the point $B_L = 0$. We calculated the normalized reconnection rate as 0.064 for MMS2 by $R = E_M / \left(V_{AeL} B_L\right)$, where V_{AeL} is the electron Alfvén speed, and B_L is the L component of the average magnetic field. The normalized reconnection rate is about 1/3 of the estimated aspect ratio of EDR (<0.2), probably suggesting a longer EDR along the $\mathbf{L}$ direction.

To investigate the role of $E_\parallel$ in electron dynamics, we plotted electron velocity distributions presented in the $V_\mathbf{b} - V_{(\mathbf{b}\times\mathbf{v})\times\mathbf{b}}$ plane in Figures 3f and 3g. The distributions are selected at two sides of the EDR (times marked by the arrows in Figure 3b), where MMS observed beam populations along the parallel direction (Figures 3f and 3g). The beam energy is ~180 eV on the $B_L > 0$ side and ~60 eV on the $B_L < 0$ side. The beam seems to
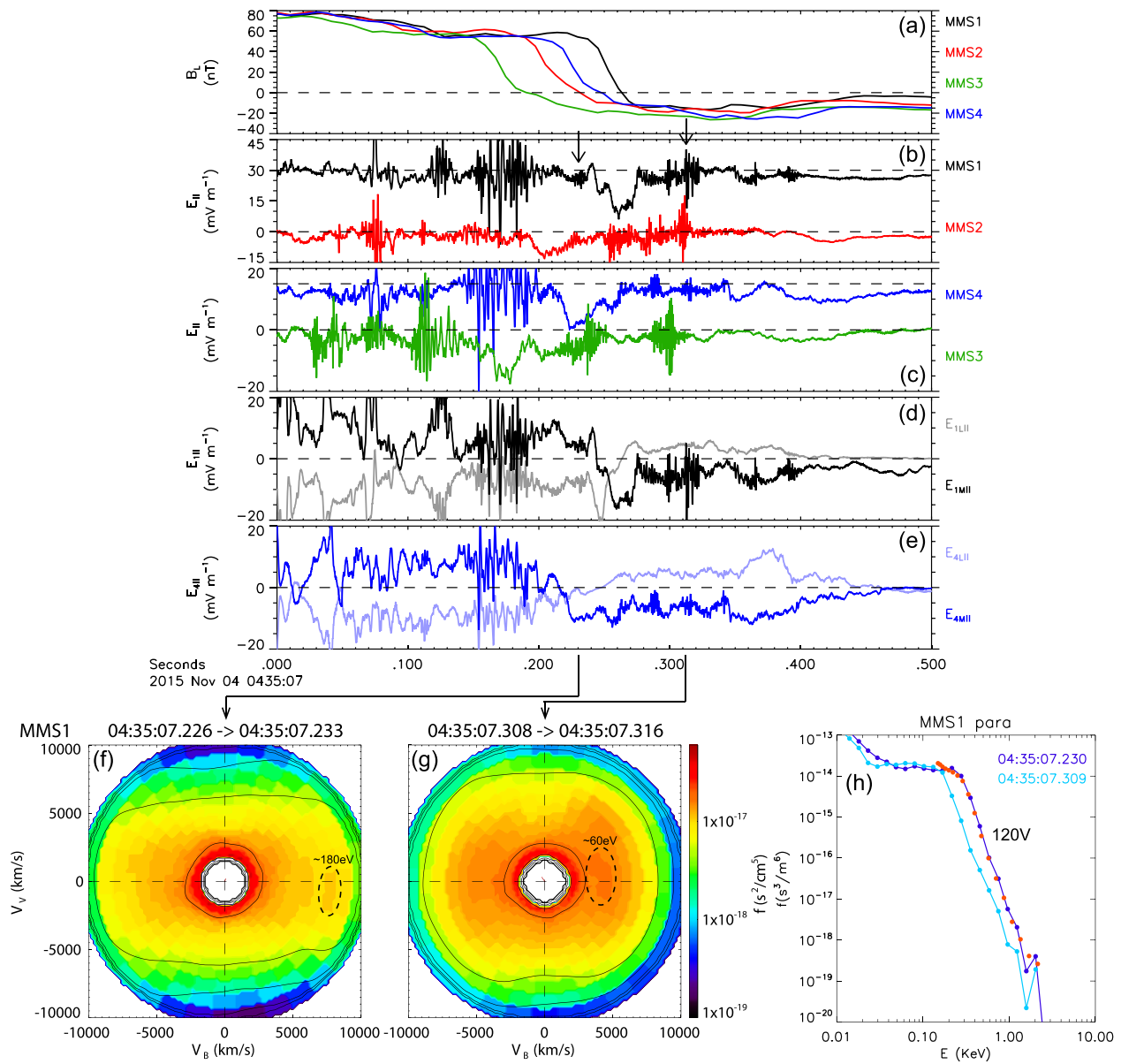
Figure 3. Parallel electric fields observed by four Magnetospheric Multiscale (MMS) spacecraft. (a) Magnetic field B_L, (b and c) parallel electric fields, (d and e) parallel components of the electric field E_L and E_M from MMS1 and MMS4, respectively, (f and g) electron distribution function in the $V_{\mathbf{b}} - V_{(\mathbf{b}\times\mathbf{v})\times\mathbf{b}}$ plane, and (h) parallel electron phase space density f.

be accelerated by the $E_\parallel$ when passing through the EDR and the potential is ∼120 V, consistent with the electric potential calculated by the $E_\parallel$ profile. We also calculated the acceleration potential by comparing the parallel electron phase space density f at two sides (Figure 3h). Using Liouville's theorem by assuming $df/dt = 0$ along the electron trajectory, a potential of 120 V was obtained. It seems that the $E_\parallel$ inside the EDR generates a potential of 120 V, which can accelerate electrons passing through it. In the inflow region with higher potential, MMS observed many bipolar $E_\parallel$ structures (Figures 3b and 3c), which is the typical signature of electron holes (Cattell et al., 2005; Drake et al., 2003). This is similar to previous observations of electron holes generated at the high-potential side of the double layer (Ergun et al., 2009; Wang et al., 2014). In these cases, the electron holes are formed due to the instability of the high-energy electron beam (Newman et al., 2001).

5. Electron Heating in CS

As shown in Figure 1i, electron heating is clearly visible in the CS. Between 04:35:06.95 and 04:35:07.23 UT, when MMS intersected the lower CS (below the pale dashed line in Figure 2k), electrons were heated in the parallel direction from 70 to 160 eV, whereas no heating was observed in the perpendicular direction (Figure 1i). In contrast, the parallel electron heating was smaller in the upper CS (04:35:07.28–04:35:07.50 UT), from 95 to 120 eV. The parallel electron heating can also be seen in the electron pitch angle distributions. In the broad CS, electrons were highly anisotropic, having enhanced fluxes near pitch angles of 0° and 180° (Figures 4d and 4e and 4i and 4j).

Figure 4k shows the electron parallel phase space density f observed by MMS1. The blue and cyan dotted lines show the background distribution (04:35:06.95 UT) and inflow distribution (04:35:07.20 UT), respectively. The inflow distribution is characterized by parallel electron heating and a flat-top distribution where f was nearly
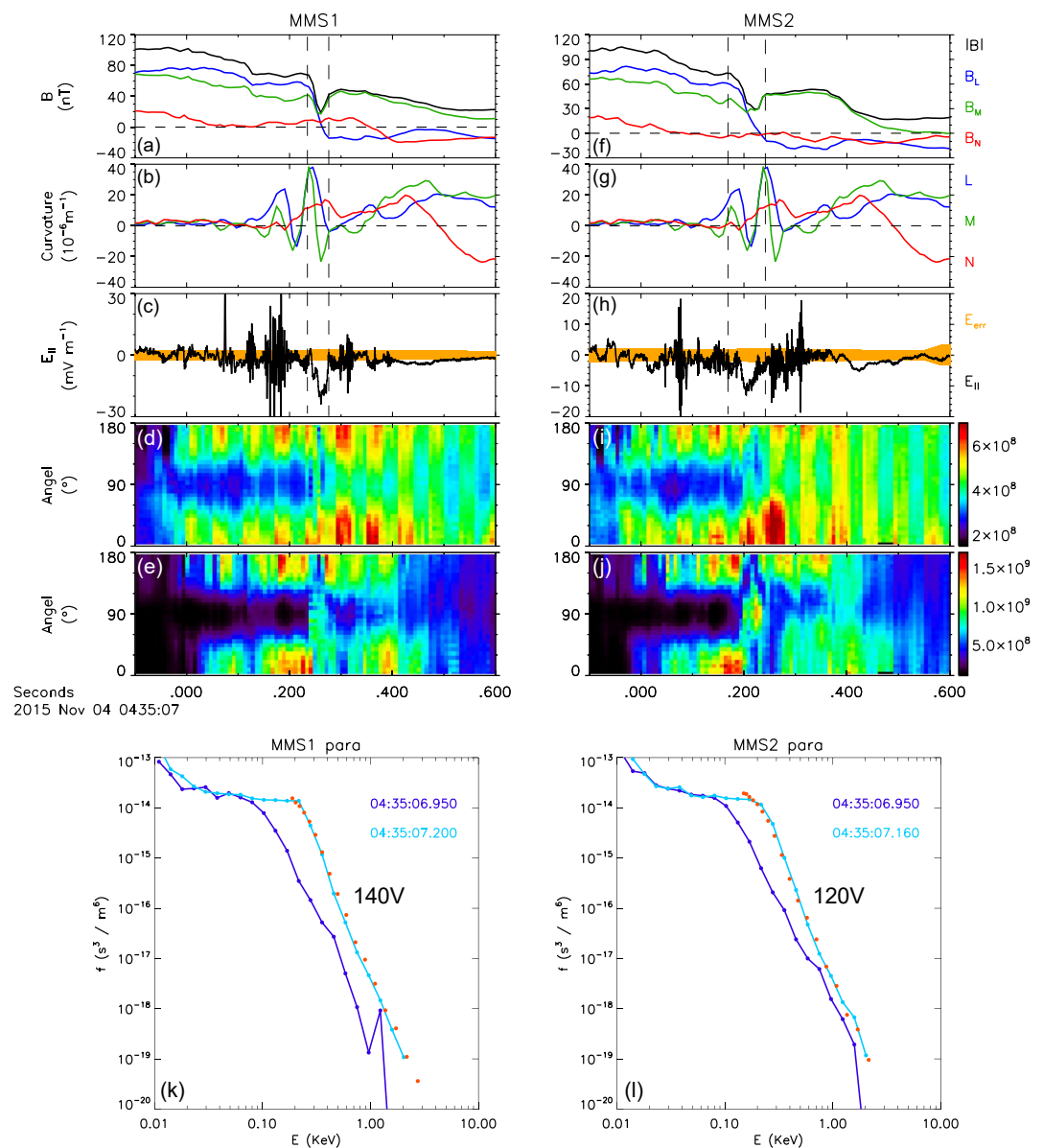

Figure 4. Magnetospheric Multiscale 1 (MMS1) observations of (a) magnetic field, (b) magnetic field curvature, (c) parallel electric field, and (d and e) electron pitch angle distributions for 0–200 eV and 0.2–2 keV respectively, with flux as keV (cm^{-2} s^{-1} sr^{-1} keV^{-1}). (f–j) The data in the same format observed by MMS2 (k and l) Parallel electron phase space density f.

constant for the energy range of 40–200 eV. These characteristics of temperature and electron distributions are consistent with the electron heating in the inflow region of asymmetric reconnection (Egedal et al., 2011; Graham et al., 2014, 2016). This parallel electron heating is thought to be generated by $E_\parallel$ that can trap and accelerate electrons (Egedal et al., 2008). To test if this mechanism is consistent with the observed heating, we estimated the parallel accelerating potential $\phi_\parallel$ needed to produce the distributions. We did not use the background $f_\parallel$ to map directly, as parallel distribution was complex, like the electron beam with an energy of 1,233 eV (the blue dot at 1,233 eV in Figure 4k). Instead, we assumed an isotropic background distribution and used the perpendicular distribution to replace the parallel distribution. This assumption is reasonable, as the background parallel and perpendicular temperatures are equal (Figure 1i) and electron velocity distribution in $V_\parallel - V_\perp$ plane is isotropic. The orange dots in Figure 4k show the mapped background distribution using a $\phi_\parallel$ of 140 V. The mapped distribution agrees well with the inflow distribution. Similarly, a $\phi_\parallel$ of 120 V was mapped using MMS2 data (Figure 4l). In contrast, in the inflow region with $B_L < 0$ (04:35:07.28–04:35:07.50 UT), the parallel heating and mapped $\phi_\parallel$ were both smaller, consistent with simulations of asymmetric reconnection (Egedal et al., 2011).

Inside the EDR (between two vertical dashed lines in Figures 4a–4c and 4f–4h), MMS observed strong fluxes enhancements near pitch angle of 0° for electrons with energy <200 eV (Figures 4d and 4i), which were caused by the negative $E_\parallel$ therein (Figures 4c and 4h). Regarding electrons with energy larger than 200 eV, fluxes near pitch angles of 0° and 180° decreased dramatically, while having significant increases near 90° (Figures 4e and 4j). Note that the electron fluxes enhancement near 90° inside the EDR is not caused by the pitch angle diffusion, as the electron distributions here were not isotropic. If pitch angle scattering occurs at one location along a magnetic flux tube, the trapped electrons should become isotropic along the entire length of the flux tube (Egedal et al., 2016). Thus, the observations of $T_{e\parallel} \gg T_{e\perp}$ just outside the EDR show that the electron magnetic moments μ should be conserved as the electrons pass through the EDR. The reason why the electron perpendicular fluxes were enhanced inside the EDR can be explained by the expression for the μ. As shown in Equation 31 of Littlejohn (1983), magnetic moment $\mu = mv_\perp^2/2B$ is only the first term in an expansion for this adiabatic invariant. In locations of strong magnetic curvature, higher order terms of μ become important. Inside the EDR, magnetic curvature was indeed large (Figures 4b and 4g), consistent with the discussion.

6. Discussion and Conclusions

We have investigated an electron-scale magnetosheath reconnection event using MMS data. MMS crossed a super-Alfvénic electron jet embedded in a broad CS. The width of this broad CS is ∼103.1 km (∼147.3 d_e), much thicker than the electron jet (∼11.7 d_e). The jet structure was identified as the EDR, characterized by the intense out-of-plane current, Hall electric field, $E_\parallel$, and $\mathbf{J} \cdot \mathbf{E}' > 0$. Based on the four MMS satellites observations, this EDR was located at a distance of >19.4 km (27.7 d_e) downstream of the X-line, implying an EDR extending to the exhaust. This extended EDR is similar to recent simulation results (Le et al., 2013). The strong electron pressure anisotropy in the broad CS suggests that the current of the EDR could be generated by the firehose instability.

In this letter, the reconnection event is a typical asymmetric reconnection with a large guide field. This event is different from most magnetosheath reconnecting CSs that are usually symmetric (Eriksson et al., 2018; Phan et al., 2018; Wilder et al., 2017). The asymmetry of the magnetic field and plasma on two sides of the CS can cause the inflow speed on the larger $|\mathbf{B}|$ side to be negligible (Pritchett, 2008), which is consistent with our observations. The results of our observations are important supplements to the reconnection study under different magnetic field and plasma conditions.

A remarkable feature in this CS is the large-amplitude and unipolar $E_\parallel$ that had a wide distribution inside the EDR. This $E_\parallel$ was observed by four spacecraft across the whole EDR crossing, suggesting that $E_\parallel$ could wrap the X-line. Simulations with large system size have shown that $E_\parallel$ has a wide spatial extent that fills the entire diffusion region (Egedal et al., 2012). Our observations support this conclusion and show that even in a small-scale CS where ions are not coupled, $E_\parallel$ had a large spatial distribution around the X-line. We have examined other reported MMS magnetosheath reconnecting events (e.g., Eriksson et al., 2018; Phan et al., 2018; Voros et al., 2017; Wilder et al., 2017, 2018), and found that $E_\parallel$ seems a common feature in these events that usually have strong guide fields. More statistical work is needed to reveal this universality. The differences of the duration and amplitude of $E_\parallel$ observed by four spacecraft indicate that the $E_\parallel$ distribution was not uniform inside the EDR. The potential drop of this $E_\parallel$ is about 120 V, and the high-potential side is in the inflow region with larger $|\mathbf{B}|$ side. The $E_\parallel$ is found to

accelerate electrons passing through the EDR and generates electron beams with higher energy. These high-energy electron beams can cause many bipolar $E_\parallel$ structures, or electron holes, which can trap and accelerate the electrons, in the inflow region with higher potential (Egedal et al., 2005; Eriksson et al., 2018; Graham et al., 2016).

In conclusion, MMS crossed a strong electron jet embedded in a broad CS. This electron jet structure was identified as an extended EDR, characterized by the intense out-of-plane current, super-Alfvénic electron outflow, $E_\parallel$, and $\mathbf{J} \cdot \mathbf{E'} > 0$. The large-amplitude and unipolar $E_\parallel$ was observed inside the whole EDR interval by four spacecraft, indicating that this $E_\parallel$ structure can fill the entire EDR, which has been rarely reported in spacecraft observations. This large-scale $E_\parallel$ is important for electron heating and acceleration inside the EDR. Our observations suggest that $E_\parallel$ can dominate the electron dynamics inside the EDR of magnetosheath reconnection due to its large spatial distribution. Future work is needed to reveal whether this $E_\parallel$ structure is general for magnetosheath reconnection events that usually have large guide fields and small dimensions.

Data Availability Statement

The MMS data set in this work are publicly available from the MMS Science Data Center (https://lasp.colorado.edu/mms/sdc/public/about/browse-wrapper/). The data from different spacecraft (MMS1-4) and instruments (FGM for magnetic field, EDP for electric field, and FPI for plasma) can be downloaded in the subdirectory of the link provided.

References

Burch, J. L., Moore, T. E., Torbert, R. B., & Giles, B. L. (2016). Magnetospheric multiscale overview and science objectives. *Space Science Reviews*, *199*(1–4), 5–21. https://doi.org/10.1007/s11214-015-0164-9

Burch, J. L., Torbert, R. B., Phan, T. D., Chen, L.-J., Moore, T. E., Ergun, R. E., et al. (2016). Electron-scale measurements of magnetic reconnection in space. *Science*, *352*(6290), aaf2939. https://doi.org/10.1126/science.aaf2939

Cattell, C., Dombeck, J., Wygant, J., Drake, J. F., Swisdak, M., Goldstein, M. L., et al. (2005). Cluster observations of electron holes in association with magnetotail reconnection and comparison to simulations. *Journal of Geophysical Research*, *110*(A1), A01211. https://doi.org/10.1029/2004ja010519

Drake, J. F., Shay, M. A., Thongthai, W., & Swisdak, M. (2005). Production of energetic electrons during magnetic reconnection. *Physical Review Letters*, *94*(9), 095001. https://doi.org/10.1103/PhysRevLett.94.095001

Drake, J. F., Swisdak, M., Cattell, C., Shay, M. A., Rogers, B. N., & Zeiler, A. (2003). Formation of electron holes and particle energization during magnetic reconnection. *Science*, *299*(5608), 873–877. https://doi.org/10.1126/science.1080333

Egedal, J., Daughton, W., & Le, A. (2012). Large-scale electron acceleration by parallel electric fields during magnetic reconnection. *Nature Physics*, *8*(4), 321–324. https://doi.org/10.1038/Nphys2249

Egedal, J., Fox, W., Katz, N., Porkolab, M., Oieroset, M., Lin, R. P., et al. (2008). Evidence and theory for trapped electrons in guide field magnetotail reconnection. *Journal of Geophysical Research-Space Physics*, *113*(A12), A12207. https://doi.org/10.1029/2008ja013520

Egedal, J., Le, A., Pritchett, P. L., & Daughton, W. (2011). Electron dynamics in two-dimensional asymmetric anti-parallel reconnection. *Physics of Plasmas*, *18*(10), 102901. https://doi.org/10.1063/1.3646316

Egedal, J., Oieroset, M., Fox, W., & Lin, R. P. (2005). In situ discovery of an electrostatic potential, trapping electrons and mediating fast reconnection in the earth's magnetotail. *Physical Review Letters*, *94*(2), 025006. https://doi.org/10.1103/PhysRevLett.94.025006

Egedal, J., Wetherton, B., Daughton, W., & Le, A. (2016). Processes setting the structure of the electron distribution function within the exhausts of anti-parallel reconnection. *Physics of Plasmas*, *23*(12), 122904. https://doi.org/10.1063/1.4972135

Ergun, R. E., Andersson, L., Tao, J., Angelopoulos, V., Bonnell, J., McFadden, J. P., et al. (2009). Observations of double layers in Earth's plasma sheet. *Physical Review Letters*, *102*(15), 155002. https://doi.org/10.1103/PhysRevLett.102.155002

Ergun, R. E., Goodrich, K. A., Wilder, F. D., Holmes, J. C., Stawarz, J. E., Eriksson, S., et al. (2016). Magnetospheric multiscale satellites observations of parallel electric fields associated with magnetic reconnection. *Physical Review Letters*, *116*(23), 235102. https://doi.org/10.1103/PhysRevLett.116.235102

Ergun, R. E., Tucker, S., Westfall, J., Goodrich, K. A., Malaspina, D. M., Summers, D., et al. (2016). The axial double probe and fields signal processing for the MMS mission. *Space Science Reviews*, *199*(1–4), 167–188. https://doi.org/10.1007/s11214-014-0115-x

Eriksson, E., Vaivads, A., Graham, D. B., Divin, A., Khotyaintsev, Y. V., Yordanova, E., et al. (2018). Electron energization at a reconnecting magnetosheath current sheet. *Geophysical Research Letters*, *45*(16), 8081–8090. https://doi.org/10.1029/2018gl078660

Eriksson, S., Wilder, F. D., Ergun, R. E., Schwartz, S. J., Cassak, P. A., Burch, J. L., et al. (2016). Magnetospheric multiscale observations of the electron diffusion region of large guide field magnetic reconnection. *Physical Review Letters*, *117*(1), 015001. https://doi.org/10.1103/PhysRevLett.117.015001

Graham, D. B., Khotyaintsev, Y. V., Norgren, C., Vaivads, A., André, M., Lindqvist, P. A., et al. (2016). Electron currents and heating in the ion diffusion region of asymmetric reconnection. *Geophysical Research Letters*, *43*(10), 4691–4700. https://doi.org/10.1002/2016gl068613

Graham, D. B., Khotyaintsev, Y. V., Vaivads, A., Andre, M., & Fazakerley, A. N. (2014). Electron dynamics in the diffusion region of an asymmetric magnetic reconnection. *Physical Review Letters*, *112*(21), 215004. https://doi.org/10.1103/PhysRevLett.112.215004

Hesse, M., & Cassak, P. A. (2020). Magnetic reconnection in the space sciences: Past, present, and future. *Journal of Geophysical Research-Space Physics*, *125*(2), e2018JA025935. https://doi.org/10.1029/2018JA025935

Huang, C., Lu, Q. M., & Wang, S. (2010). The mechanisms of electron acceleration in antiparallel and guide field magnetic reconnection. *Physics of Plasmas*, *17*(7), 072306. https://doi.org/10.1063/1.3457930

Karimabadi, H., Roytershteyn, V., Vu, H. X., Omelchenko, Y. A., Scudder, J., Daughton, W., et al. (2014). The link between shocks, turbulence, and magnetic reconnection in collisionless plasmas. *Physics of Plasmas*, *21*(6), 062308. https://doi.org/10.1063/1.4882875

Le, A., Egedal, J., Ohia, O., Daughton, W., Karimabadi, H., & Lukin, V. S. (2013). Regimes of the electron diffusion region in magnetic reconnection. *Physical Review Letters*, *110*(13), 135004. https://doi.org/10.1103/PhysRevLett.110.135004

Li, X. M., Wang, R. S., Lu, Q. M., Hwang, Y. O. O., Zong, Q. G., Russell, C. T., & Wang, S. (2019). Observation of nongyrotropic electron distribution across the electron diffusion region in the magnetotail reconnection. *Geophysical Research Letters*, *46*(24), 14263–14273. https://doi.org/10.1029/2019gl085014

Lindqvist, P. A., Olsson, G., Torbert, R. B., King, B., Granoff, M., Rau, D., et al. (2016). The spin-plane double probe electric field instrument for MMS. *Space Science Reviews*, *199*(1–4), 137–165. https://doi.org/10.1007/s11214-014-0116-9

Littlejohn, R. G. (1983). Variational principles of guiding center motion. *Journal of Plasma Physics*, *29*(1), 111–125. https://doi.org/10.1017/S002237780000060x

Lu, Q. M., Wang, H. Y., Wang, X. Y., Lu, S., Wang, R. S., Gao, X. L., & Wang, S. (2020). Turbulence-driven magnetic reconnection in the magnetosheath downstream of a quasi-parallel shock: A three-dimensional global hybrid simulation. *Geophysical Research Letters*, *47*(1), e2019GL085661. https://doi.org/10.1029/2019GL085661

Montag, P. (2018). *Modeling the formation of current sheets in symmetric and asymmetric reconnection, PhD thesis*. Massachusetts Institute of Technology. Retrieved from https://dspace.mit.edu/handle/1721.1/119927

Newman, D. L., Goldman, M. V., Ergun, R. E., & Mangeney, A. (2001). Formation of double layers and electron holes in a current-driven space plasma. *Physical Review Letters*, *87*(25), 255001. https://doi.org/10.1103/PhysRevLett.87.255001

Phan, T. D., Drake, J. F., Shay, M. A., Mozer, F. S., & Eastwood, J. P. (2007). Evidence for an elongated (>60 ion skin depths) electron diffusion region during fast magnetic reconnection. *Physical Review Letters*, *99*(25), 255002. https://doi.org/10.1103/PhysRevLett.99.255002

Phan, T. D., Eastwood, J. P., Shay, M. A., Drake, J. F., Sonnerup, B. U. Ö., Fujimoto, M., et al. (2018). Electron magnetic reconnection without ion coupling in Earth's turbulent magnetosheath. *Nature*, *557*(7704), 202–206. https://doi.org/10.1038/s41586-018-0091-5

Pollock, C., Moore, T., Jacques, A., Burch, J., Gliese, U., Saito, Y., et al. (2016). Fast plasma investigation for magnetospheric multiscale. *Space Science Reviews*, *199*(1–4), 331–406. https://doi.org/10.1007/s11214-016-0245-4

Pritchett, P. L. (2008). Collisionless magnetic reconnection in an asymmetric current sheet. *Journal of Geophysical Research*, *113*(A6), A06210. https://doi.org/10.1029/2007ja012930

Pritchett, P. L., & Coroniti, F. V. (2004). Three-dimensional collisionless magnetic reconnection in the presence of a guide field. *Journal of Geophysical Research*, *109*(A1), A01220. https://doi.org/10.1029/2003ja009999

Rager, A. C., Dorelli, J. C., Gershman, D. J., Uritsky, V., Avanov, L. A., Torbert, R. B., et al. (2018). Electron crescent distributions as a manifestation of diamagnetic drift in an electron-scale current sheet: Magnetospheri 7.5 ms fast plasma investigation moments. *Geophysical Research Letters*, *45*(2), 578–584. https://doi.org/10.1002/2017gl076260

Retino, A., Sundkvist, D., Vaivads, A., Mozer, F., Andre, M., & Owen, C. J. (2007). In situ evidence of magnetic reconnection in turbulent plasma. *Nature Physics*, *3*(4), 235–238. https://doi.org/10.1038/nphys574

Ricci, P., Brackbill, J. U., Daughton, W., & Lapenta, G. (2004). Collisionless magnetic reconnection in the presence of a guide field. *Physics of Plasmas*, *11*(8), 4102–4114. https://doi.org/10.1063/1.1768552

Russell, C. T., Anderson, B. J., Baumjohann, W., Bromund, K. R., Dearborn, D., Fischer, D., et al. (2016). The Magnetospheric multiscale magnetometers. *Space Science Reviews*, *199*(1–4), 189–256. https://doi.org/10.1007/s11214-014-0057-3

Schwartz, S. J. (1998). Shock and discontinuity normals, mach numbers and related parameters. In G. Paschmann, & P. W. Daly (Eds.), *Analysis methods for multi-spacecraft data* (Vol. 1, pp. 249–270). International Space Science Institute.

Swisdak, M., Drake, J. F., Shay, M. A., & McIlhargey, J. G. (2005). Transition from antiparallel to component magnetic reconnection. *Journal of Geophysical Research*, *110*(A5), A05210. https://doi.org/10.1029/2004ja010748

Torbert, R. B., Burch, J. L., Phan, T. D., Hesse, M., Argall, M. R., Shuster, J., et al. (2018). Electron-scale dynamics of the diffusion region during symmetric magnetic reconnection in space. *Science*, *362*(6421), 1391–1395. https://doi.org/10.1126/science.aat2998

Voros, Z., Yordanova, E., Varsani, A., Genestreti, K. J., Khotyaintsev, Y. V., Li, W., et al. (2017). MMS observation of magnetic reconnection in the turbulent magnetosheath. *Journal of Geophysical Research: Space Physics*, *122*(11), 11442–11467. https://doi.org/10.1002/2017ja024535

Wang, R. S., Lu, Q., Khotyaintsev, Y. V., Volwerk, M., Du, A., Nakamura, R., et al. (2014). Observation of double layer in the separatrix region during magnetic reconnection. *Geophysical Research Letters*, *41*(14), 4851–4858. https://doi.org/10.1002/2014gl061157

Wang, R. S., Lu, Q. M., Lu, S., Russell, C. T., Burch, J. L., Gershman, D. J., et al. (2020). Physical implication of two types of reconnection electron diffusion regions with and without ion-coupling in the magnetotail current sheet. *Geophysical Research Letters*, *47*(21), e2020GL088761. https://doi.org/10.1029/2020GL088761

Wang, R. S., Nakamura, R., Lu, Q., Baumjohann, W., Ergun, R. E., Burch, J. L., et al. (2017). Electron-scale quadrants of the hall magnetic field observed by the magnetospheric multiscale spacecraft during asymmetric reconnection. *Physical Review Letters*, *118*(17), 175101. https://doi.org/10.1103/PhysRevLett.118.175101

Wang, S. M., Wang, R. S., Lu, Q. M., Burch, J. L., & Wang, S. (2021). Energy dissipation via magnetic reconnection within the coherent structures of the magnetosheath turbulence. *Journal of Geophysical Research-Space Physics*, *126*(4), e2020JA028860. https://doi.org/10.1029/2020JA028860

Wang, S. M., Wang, R. S., Lu, Q. M., Fu, H. S., & Wang, S. (2020). Direct evidence of secondary reconnection inside filamentary currents of magnetic flux ropes during magnetic reconnection. *Nature Communications*, *11*(1), 3964. https://doi.org/10.1038/s41467-020-17803-3

Wilder, F. D., Ergun, R. E., Burch, J. L., Ahmadi, N., Eriksson, S., Phan, T. D., et al. (2018). The role of the parallel electric field in electron-scale dissipation at reconnecting currents in the magnetosheath. *Journal of Geophysical Research: Space Physics*, *123*(8), 6533–6547. https://doi.org/10.1029/2018ja025529

Wilder, F. D., Ergun, R. E., Eriksson, S., Phan, T. D., Burch, J. L., Ahmadi, N., et al. (2017). Multipoint measurements of the electron jet of symmetric magnetic reconnection with a moderate guide field. *Physical Review Letters*, *118*(26), 265101. https://doi.org/10.1103/PhysRevLett.118.265101

Yamada, M., Kulsrud, R., & Ji, H. T. (2010). Magnetic reconnection. *Reviews of Modern Physics*, *82*(1), 603–664. https://doi.org/10.1103/RevModPhys.82.603

Yordanova, E., Vörös, Z., Varsani, A., Graham, D. B., Norgren, C., Khotyaintsev, Y. V., et al. (2016). Electron scale structures and magnetic reconnection signatures in the turbulent magnetosheath. *Geophysical Research Letters*, *43*(12), 5969–5978. https://doi.org/10.1002/2016gl069191